

Reinforcement Learning for Legged Robots: Motion Imitation from Model-Based Optimal Control

AJ Miller[†], Shamel Fahmi[†], Matthew Chignoli, and Sangbae Kim*

Abstract—We propose **MIMOC**: Motion Imitation from Model-Based Optimal Control. **MIMOC** is a **Reinforcement Learning (RL)** controller that learns agile locomotion by imitating reference trajectories from model-based optimal control. **MIMOC** mitigates challenges faced by other motion imitation **RL** approaches because the references are dynamically consistent, require no motion retargeting, and include torque references. Hence, **MIMOC** does not require fine-tuning. **MIMOC** is also less sensitive to modeling and state estimation inaccuracies than model-based controllers. We validate **MIMOC** on the Mini-Cheetah in outdoor environments over a wide variety of challenging terrain, and on the MIT Humanoid in simulation. We show cases where **MIMOC** outperforms model-based optimal controllers, and show that imitating torque references improves the policy’s performance.

I. INTRODUCTION

Legged robots have shown remarkable agile capabilities in academia [1]–[6] and in industry [7]–[9]. Locomotion control for legged robots usually relies on model-based optimal control approaches such as **Whole-Body Control (WBC)** [10]–[12], **Model Predictive Control (MPC)** [13]–[15], and **Trajectory Optimization (TO)** [16]–[19]. Recently, **Reinforcement Learning (RL)** for locomotion control has proven to be robust and reliable [20]–[25]. To date, no dominant approach among model-based, **RL**, or hybrid methods has emerged in the field of legged robots.

Model-based approaches originate from physics and are interpretable, allowing a skilled engineer to directly evaluate and debug controllers. **RL** approaches typically lack a model and are more challenging to interpret, design, and tune. However, they are also less sensitive to model inaccuracies. A major advantage of **RL** is that the agent learns from its mistakes during training. Simulated noisy observations and randomized physical parameters of the robot and the environment teach the policy to overcome modeling and state estimation inaccuracies better than model-based approaches.

In this work, we propose **Motion Imitation from Model-Based Optimal Control (MIMOC)**, an **RL** locomotion controller. **MIMOC** combines the best of both worlds by using model-based optimal control to guide the **RL** policy. We train our policies to imitate rich reference trajectories from model-based optimal controllers [10], [15]. The **RL** policy trains with simple, minimally-tuned rewards. To transfer the policy on hardware as shown in Fig. 1, we train on a range of sensor noise, body masses, and disturbances.



Fig. 1. This figure shows multiple screenshots of **MIMOC** running on the Mini-Cheetah in outdoor environments. Mini-Cheetah was able to traverse different terrains with different slopes and friction including grass, rocks, asphalt, mud, etc. The full experiments can be found in Video 5.

II. RELATED WORK

In **RL** for legged robots, the policy requires some inductive bias or prior knowledge. One way is to introduce a gait dependency. This is usually referred to as **Policies Modulating Trajectory Generators (PMTGs)** [1], [26], where the prior is enforced via **Central Pattern Generators (CPGs)**, and the policy then modulates the parameters of the **CPG**, such as stepping frequency. The main drawback of this approach is the explicit gait dependency; the gait is not an emergent behavior but is rather transcribed by the **CPG**. Another way to use priors is via reward shaping [20], [27], [28]. Here, the policy does not depend on a specific gait and several gaits may emerge. However, the issue is the rewards are handcrafted, may be complicated, and require tedious tuning.

Another common approach is to learn locomotion by imitating motion from animals or animal-like characters [29]–[32]. The prior knowledge is encoded via reference motions the policy is rewarded for tracking. These reference motions are obtained either from animated motion data, **Motion Capture (MoCap)** data, or from video clips of animals and humans. The reference motions are then retargeted to fit the morphology of the legged robot.

Despite learning different locomotion skills on real legged robots, **RL** via motion imitation poses several challenges. One challenge is in acquiring data, especially **MoCap** data. It is especially hard to acquire animal **MoCap** data versus human data [31]. Additionally, motion retargeting poses another issue since the morphology of humans and animals are different from humanoid and quadruped robots. Thus,

[†]Equal contribution. *The authors are with the Biomimetic Robotics Lab, Massachusetts Institute of Technology (MIT), Cambridge, MA, USA. (email: {sfahmi, ajm4, chignoli}@mit.edu).

the retargeted motion may not be kinematically accurate. Finally, there is no guarantee this motion reference data is dynamically feasible on a legged robot [29].

III. PROPOSED APPROACH AND CONTRIBUTION

MIMOC is an **RL** locomotion controller that learns from model-based optimal control. Unlike other motion imitation **RL** controllers that rely on **MoCap** or video clips, **MIMOC** relies on the reference trajectories provided by model-based controllers. Thus, **MIMOC** does not require any motion retargeting since the reference trajectories are robot-specific. Model-based optimal controllers may consider the robot’s full whole-body kinematics and dynamics, unlike **MoCap** or video clips, to create dynamically feasible reference trajectories. The reference trajectories can come from many **TO**-based planners similar to [19], [33]. We can provide **MIMOC** with different labeled locomotion skill references including walking and jumping. This is an advantage over human or animal data since from **MoCap** data is highly unstructured and difficult to parameterize [31].

Learning from model-based controllers provides us with torque references which are not included in **MoCap** or video clips. This is advantageous for dynamic locomotion where controlling torques and **Ground Reaction Forces (GRFs)** is essential [34]. To elaborate, the robot must balance itself by generating contact forces through torques which kinematic references do not provide [34], [35]. Torque references give the robot an idea of the forces it should generate when it is in contact. Since our reference trajectories are dynamically feasible and provide **MIMOC** with torque references, transferring the policy to real platforms does not require extensive domain adaptation or reward shaping and tuning.

MIMOC not only overcomes the challenges of **RL** via motion imitation but also the challenges that arise from model-based controllers. Model-based approaches rely heavily on state estimation which is known to have noise issues [36]. We train **MIMOC** with sensor noise to make the policy less sensitive to noisy state estimation. We also train our agent on a range of environments and robot physical parameters to make it more robust than the model-based controller.

Similar to **MIMOC**, other **RL** controllers imitate reference motions from model-based controllers [37]–[39]. Babadi et al. [37] proposed imitating references from a Monte Carlo-based planner and evaluated this approach on bipedal and quadrupedal characters. Li et al. [38] relied on a hybrid-zero-dynamics-based planner to generate the motion references and evaluated this approach on the Cassie bipedal robot. Brakel et al. [39] proposed a centroidal-dynamics model-based planner to generate the motion references and tested this approach on the ANYmal quadruped robot. **MIMOC** differs from the aforementioned works in several aspects.

First, the work in [37]–[39] does not include torque reward tracking, which we demonstrate as valuable in producing high-quality policies on the real robot. Second, the policies in [38], [39] require motion references (future and past motion frames) as observations. Thus, these policies are restricted to the reference trajectory behaviors on deployment

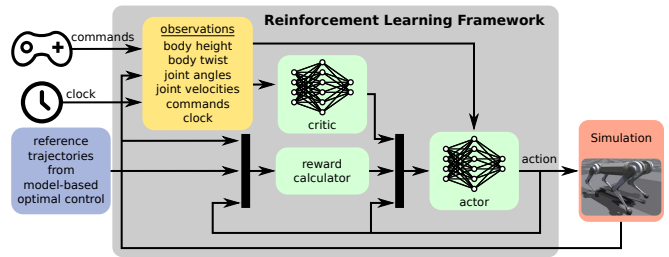


Fig. 2. The **RL** framework used to train **MIMOC**’s policy.

and are unable to generalize beyond that. On the other hand, **MIMOC** uses the reference trajectories only to reward the policy and to initialize each episode; not as observations. As a result, **MIMOC** does need a gait library or a reference generator when deployed. Additionally, **MIMOC** shows that motion references are not needed as observations, which reduces the input size of the policy’s network.

Third, in this work, the reference trajectories do not come directly from model-based optimization. Instead, we run our model-based controllers in a highly accurate dynamic simulator and use the resulting motion of the robot as the reference. This provides us highly accurate, dynamically feasible references. Finally, the work in [39] was tested only on a single robot in simulation, the work in [37] was not tested on hardware, and the work in [38] was tested only on a bipedal robot. In this work, we test **MIMOC** on the MIT Humanoid [40] and the Mini-Cheetah [4] in two different simulation environments: IsaacGym [41], and Cheetah-Software [42]. We also test **MIMOC** on the Mini-Cheetah hardware.

IV. METHOD

The goal of **MIMOC** is to learn a locomotion controller that tracks user commands by imitating model-based optimal control reference trajectories. An overview of the **RL** framework used during training is shown in Fig. 2. The reference trajectories are only used for reward computation and episode initialization for training. The policy takes the observed robot states and commands as input and outputs joint position set points that are sent to the joint-level feedback controller. Unlike [29] and [39], respectively, **MIMOC** is trained without motion retargeting and domain adaptation and also without fine-tuning.

A. Model-Based Optimal Control Reference Trajectories

The reference trajectories for the Mini-Cheetah and the MIT Humanoid are generated from the model-based framework in [10]. It includes an **MPC** and a **WBC** running hierarchically at different update rates. We collect the reference trajectories by simulating the controllers in the Cheetah-Software simulator given a range of scripted commands and using the ground truth robot states. We use Cheetah-Software [42] because it accounts for the dynamic effects of the robot’s motors and is thus more accurate than generic simulators.

To generate the reference trajectories, we collect the robot’s state $s \in \mathbb{R}^{3n+12+2n_e}$, the phase clock $\phi \in \mathbb{R}$, and the commands $c \in \mathbb{R}^3$ at every time step t . The robot state is defined as

$$s = [q^T \quad \dot{q}^T \quad \tau^T \quad x^T \quad \dot{x}^T \quad \theta^T \quad \omega^T \quad e^T \quad \dot{e}^T]^T \quad (1)$$

where $q \in \mathbb{R}^n$, $\dot{q} \in \mathbb{R}^n$, and $\tau \in \mathbb{R}^n$ are the vectors of joint positions, velocities, and torques, respectively, and n is the number of joints. The vectors $x \in \mathbb{R}^3$, $\dot{x} \in \mathbb{R}^3$, $\theta \in \mathbb{R}^3$, and $\omega \in \mathbb{R}^3$ are the body (floating base) positions, linear velocities, orientation in Cardan angles (roll-pitch-yaw), and angular velocities, respectively. The vectors $e \in \mathbb{R}^{n_e}$, $\dot{e} \in \mathbb{R}^{n_e}$ are the end-effector positions and velocities, respectively, and n_e is the number of end-effector degrees of freedom (number of end-effectors multiplied by the number of degrees of freedom per end effector). Finally, the commands $c = [c_{vx}, c_{vy}, c_{\dot{\psi}}] \in \mathbb{R}^3$ are the body forward velocity, lateral velocity, and yaw rate, respectively.

The commands are scripted to move the robot in this order: forward then backward with a longitudinal velocity of $\pm \bar{c}_{vx}$, leftwards then rightwards with a lateral velocity of $\pm \bar{c}_{vy}$, anti-clockwise then clockwise with a yaw rate of $\pm \bar{c}_{\dot{\psi}}$. The values of $\bar{c} = [\bar{c}_{vx}, \bar{c}_{vy}, \bar{c}_{\dot{\psi}}]$ are $[0.5, 0.2, 2.0]$ for the Mini-Cheetah and the MIT Humanoid. The final dataset consisted of a single clip of 60s for the Mini-Cheetah and 180s for the MIT Humanoid. Videos showing the generated reference trajectories for the Mini-Cheetah and the MIT Humanoid are shown in Video 6 and Video 7, respectively.

B. MIMOC’s RL Framework

MIMOC is formulated as an RL control problem [43]. The RL control policy $\pi(a|o)$ is the mapping between observations o and actions a . At each time step t , given the robot’s current observation o_t the agent samples an action a_t from the policy $\pi(a_t|o_t)$ and receives a reward $r_t = r(s_t, a_t)$ accordingly. When the action is applied to the agent, the environment emits the next observation o_{t+1} . The goal of RL is to find the optimal policy that maximizes the expected reward at each time step. We formulate our RL problem as an Actor-Critic (AC) method and solve it using Proximal Policy Optimization (PPO) [44].

Gym Environment. We used IsaacGym [41] with the Legged Gym implementation [20]. The policy is trained with 4096 simultaneous agents on flat terrain. The simulation environment runs at 500 Hz, and the action is computed every 5 time steps. Thus, the policy runs at 100 Hz.

Episode. At the beginning of an episode, the agents are initialized with a state that is randomly sampled from the reference trajectory. Instead of running the episode until the end of the trajectory, we run the episode for a length varying between 1-5 s depending on the training task.

Termination. Episodes are terminated and restarted under three conditions. First, if the length of the episode exceeds the maximum episode length. Second, if the end of the reference trajectory is reached. Third, if any robot link other than the feet collides with the ground (i.e., ground collision).

Rewards. The reward function is designed to guide the policy to track the reference trajectories during training. To track a reference trajectory is to minimize the error (deviation) between a certain robot state variable β and its corresponding desired reference β_{ref} (i.e., minimize $\beta_{\text{ref}} - \beta$). To minimize this error, we design the reward to maximize the squared exponential of this error (i.e., maximize $\exp(-\|\beta_{\text{ref}} - \beta\|^2)$). Since, the reference trajectories include the body, joint, and end-effector positions and velocities, and joint torques, we exploit all of these references in the reward function. This reward function is inspired from [29], [30]. The accumulated reward is computed as

$$r_t = r_q + r_{\dot{q}} + r_{\tau} + r_x + r_{\dot{x}} + r_{\theta} + r_{\omega} + r_e + r_{\dot{e}} \quad (2)$$

where each term maximizes the squared exponential of the error of a certain robot state variable β . The terms in (2) correspond to the robot joint position r_q , velocity $r_{\dot{q}}$, and torques r_{τ} , body position r_x , linear velocity $r_{\dot{x}}$, orientation r_{θ} , and angular velocity r_{ω} , end-effector positions r_e and velocities $r_{\dot{e}}$. Each term in the reward function is of the form of the generic reward r_{β}

$$r_{\beta} = w_{\beta} \sum_{i=1}^{n_d} \left[\exp(-\alpha_{\beta} \|\beta_{i,\text{ref}} - \beta_i\|^2) \right] \quad (3)$$

which is a weighted squared exponential function of weight w_{β} and width α_{β} . The weights w_{β} are manually tuned but the widths α_{β} are computed as

$$\alpha_{\beta} = \left(\frac{2}{\max(\beta^{\text{ref}}) - \min(\beta^{\text{ref}})} \right)^2. \quad (4)$$

The values of the weights w_{β} and widths α_{β} for Mini-Cheetah and the MIT Humanoid are in Table IV-B. We found that unit weights ($w_{\beta}=1$) were sufficient to train the policies. However, we found that increasing the weights w_{β} of the joint positions w_q and torques w_{τ} helped in reducing the training time of the MIT Humanoid policy. More importantly, we found that tuning the widths of the squared exponential rewards α_{β} was crucial. Without tuning these widths based on (4), the policies would fail to track the references.

Observations. The observations $o_t \in \mathbb{R}^{2n+1+6+3+2}$ are defined as

$$o_t = [q^T \quad \dot{q}^T \quad z^T \quad \dot{x}^T \quad \omega^T \quad c^T \quad \cos(\phi) \quad \sin(\phi)]^T \quad (5)$$

where $z \in \mathbb{R}$ is the body height, and $\cos(\phi)$ and $\sin(\phi)$ are associated with the gait phase clock ϕ . The commands $c \in \mathbb{R}^3$ come from the reference trajectories during training but are user-input during deployment. The body’s linear velocity is expressed in body-fixed frame. Finally, these observations were not normalized or scaled.

Actions and Control Law. The actions $a_t \in \mathbb{R}^n$ are defined as joint position residuals from default joint positions q_0 (i.e., the robot’s default standing configuration). Thus, the desired torques τ_d sent to the robots are computed as

$$\tau_d = k_p(k_a a_t + q_0 - q_t) - k_d \dot{q}_t \quad (6)$$

TABLE I

REWARD SCALES OF THE MINI-CHEETAH AND MIT HUMANOID.

Weight w_β	Width α_β
Cheetah	
$w_q = 1.0$	$\alpha_q = [0.1, 0.5, 0.5] \in \mathbb{R}^3$ per leg
$w_{\dot{q}} = 1.0$	$\alpha_{\dot{q}} = [15, 20, 25] \in \mathbb{R}^3$ per leg
$w_\tau = 1.0$	$\alpha_\tau = [5.0, 5.0, 8.0] \in \mathbb{R}^3$ per leg
$w_x = 1.0$	$\alpha_x = [0.02, 0.02, 0.02] \in \mathbb{R}^3$
$w_{\dot{x}} = 1.0$	$\alpha_{\dot{x}} = [0.6, 0.1, 0.5] \in \mathbb{R}^3$
$w_\theta = 1.0$	$\alpha_\theta = [0.31, 0.31, 0.31] \in \mathbb{R}^3$
$w_\omega = 1.0$	$\alpha_\omega = [3.3, 2.5, 3.7] \in \mathbb{R}^3$
$w_e = 1.0$	$\alpha_e = [0.02, 0.02, 0.02] \in \mathbb{R}^3$ per foot
$w_{\dot{e}} = 1.0$	$\alpha_{\dot{e}} = [0.6, 0.1, 0.5] \in \mathbb{R}^3$ per foot
Humanoid	
$w_q = 5.0$	$\alpha_q = [0.2, 0.3, 0.9, 0.9, 0.5, 0.2, 0.2, 0.2, 0.5] \in \mathbb{R}^9$
$w_{\dot{q}} = 1.0$	$\alpha_{\dot{q}} = [3, 5, 10, 12, 8, 8, 1, 1, 12] \in \mathbb{R}^9$ per side
$w_\tau = 10.0$	$\alpha_\tau = [10, 40, 50, 60, 20, 1, 1, 1, 1] \in \mathbb{R}^9$ per side
$w_x = 1.0$	$\alpha_x = [0.06, 0.06, 0.06] \in \mathbb{R}^3$
$w_{\dot{x}} = 1.0$	$\alpha_{\dot{x}} = [1.03, 0.59, 0.61] \in \mathbb{R}^3$
$w_\theta = 1.0$	$\alpha_\theta = [0.27, 0.29, 0.13] \in \mathbb{R}^3$
$w_\omega = 1.0$	$\alpha_\omega = [4.01, 2.98, 2.04] \in \mathbb{R}^3$
$w_e = 1.0$	$\alpha_e = [2, 0.1, 0.1, 2, 0.1, 0.1] \in \mathbb{R}^6$ per side
$w_{\dot{e}} = 1.0$	$\alpha_{\dot{e}} = [2, 1, 2, 2, 1, 2] \in \mathbb{R}^6$ per side

where k_p and k_d are the proportional and derivative gains, respectively, and k_a is the action gain. The gains used for all of the joints of the Mini-Cheetah are: $k_a = 0.25$, $k_p = 20$, and $k_d = 0.5$. Each side of the MIT Humanoid (9 joints per side - 4 arm joints and 5 leg joints) had the following gains: $k_a = 0.5$, $k_p = [60, 60, 60, 60, 40, 10, 10, 10, 10]$, and $k_d = [5, 5, 5, 5, 0.1, 0.5, 0.5, 0.5, 0.5]$.

Network Architecture. The actor and critic networks are defined as **Multi-Layer Perceptron (MLP)** networks with ELU activations and hidden dimensions of $256 \times 256 \times 256$.

Domain Randomization. We added noise to the observations with random values with a range of $[-1, 1]$ multiplied by a scale for each observation. We also randomized the terrain friction with a range of $[0.5, 1.25]$ and the robot mass with a range of $[-2, 2]$ kg. We added disturbance to the robot’s body by applying an instant change of the body linear velocity with a range of $[-1, 1]$ m/s.

Policy Training. The policies are trained using the **PPO** implementation in [20]. Mini-Cheetah is trained for as few as 500 iterations in under 10 minutes of training (on an Intel 12900K CPU and Nvidia 3080ti GPU), but we preferred training for 1500 iterations. MIT Humanoid is trained with iterations ranging between 1500 iterations and 10000 iterations. We used a learning rate of 10^{-3} , batch size of 98304, 24 steps per policy update, mini-batches of 4, value loss of 1.0, clip parameter of 0.2, entropy coefficient of 0.01, discount factor of 0.99, GAE discount factor of 0.95, and desired KL of 0.01.

Real World Deployment. The policy is evaluated on board the robot at 100 Hz. To compute the observations, we relied on a contact-based state estimator similar to the state estimator in [5]. The actions are sent to a low-level joint controller that runs at 40 kHz.

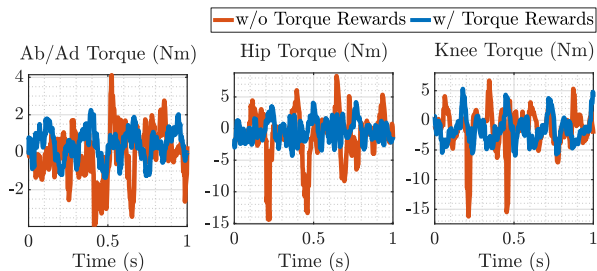


Fig. 3. The Importance of Torque Tracking Rewards. Two policies tested on the Mini-Cheetah: with versus without torque tracking rewards. The figure shows the torque values of the three joints of the right-front leg of the Mini-Cheetah in an experiment.

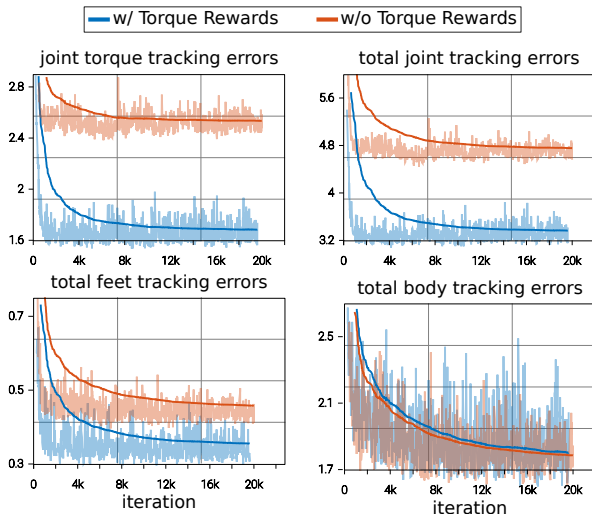


Fig. 4. The Importance of Torque Tracking Rewards. Two policies tested on the Mini-Cheetah: with versus without torque tracking rewards. The figure shows the tracking errors of the torques, and the total tracking errors of the joints, feet and body. The tracking error is defined as the mean over all agents of the difference between the robot’s current state and its corresponding reference.

V. RESULTS

We evaluate **MIMOC** on Mini-Cheetah (in simulation and experiment) and the MIT Humanoid (in simulation), and we compare **MIMOC** with the **convex MPC (cMPC)** model-based controller detailed in [10], [15]. To test our policies and compare them with the model-based controller, we used Cheetah-Software [42] because it is a more realistic simulation environment. Thus, the simulation would be one step toward real-world deployment, and we can evaluate how well can the policy be transferred to a different simulator. The videos supporting the results can be found in [45].

The Importance of Torque Tracking Rewards. **MIMOC**’s primary advantage over motion imitation from **MoCap** is that our model-based reference trajectories include torque references. We hypothesize imitating reference torques is essential for learning because controlling torques and **GRFs** are as important as controlling positions and velocities; especially during dynamic locomotion. To verify this, we compared the performance of two **MIMOC** policies: one trained with and another without torque tracking reward. We ran these policies

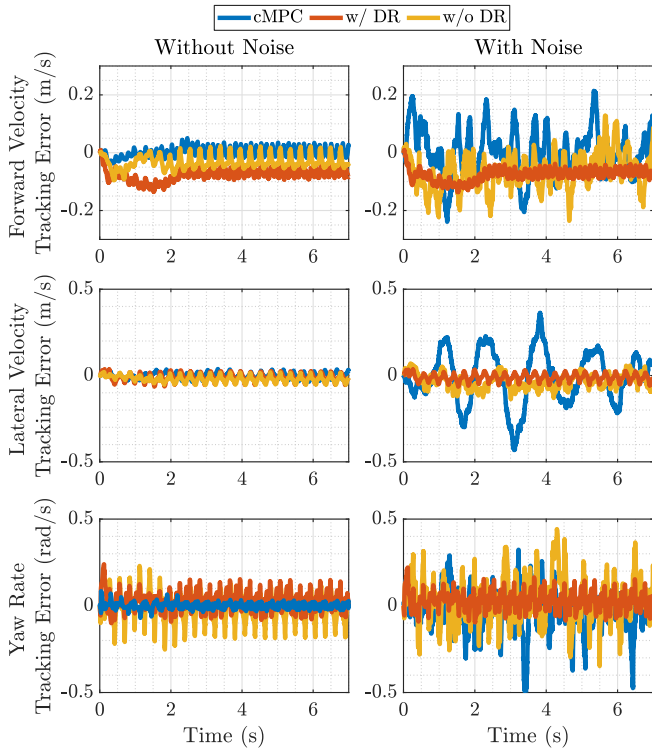


Fig. 5. Performance under Noisy State Estimation. The controllers evaluated were **MIMOC** with domain randomization, **MIMOC** without domain randomization, and model-based **cMPC**. Left: the tracking errors of the three controllers with perfect (noise-free) state estimates. Right: the tracking errors of the three controllers with noisy state estimates.

on the Mini-Cheetah as shown in Video 1. Figure 3 shows the torque values of the three joints of one leg of the Mini-Cheetah. As shown in the video, the policy trained without torque tracking rewards was shaking substantially more on the hardware. Without the torque tracking rewards, the feet had a more aggressive contact with the ground. This is also evident in Fig. 3, where the no torque tracking reward policy had higher torque peaks. Additionally, as shown in Fig. 4, when **MIMOC** is trained with torque tracking rewards, the policy learns faster with smaller tracking errors (deviations from the reference trajectories).

Performance under Noisy State Estimation. A key advantage of **RL** over model-based is that **RL** may be less sensitive to noise and/or model uncertainties, because the policy can be trained with noisy observations as part of domain randomization. To verify this, we evaluated **MIMOC** with domain randomization, **MIMOC** without domain randomization, and **cMPC** in simulation (Cheetah-Software) under noisy state estimates. To simulate noisy state estimates, we inject noise onto the robot’s body states (linear and angular position and velocity) following a normal distribution X with mean μ and standard deviation σ : $X \sim \mathcal{N}(\mu, \sigma^2)$. We used a mean $\mu = 0$ for all body states and standard deviations σ of 0.03, 0.15, 0.075, and 0.04 for the position, orientation, linear velocity, and angular velocity of the robot’s body, respectively. We commanded Mini-Cheetah to trot forward with a velocity of 0.5 m/s, once with ground truth states

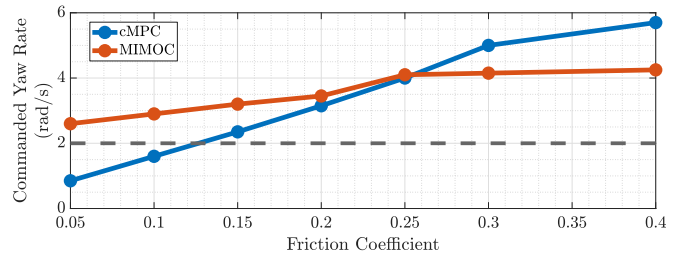


Fig. 6. Performance under Different Terrain Friction. The figure shows the maximum yaw rate command that Mini-Cheetah was able to withstand at a given friction coefficient, using **MIMOC** and **cMPC**. The dashed gray line is the maximum yaw rate that **MIMOC** was trained with.

(without noise) and once with noisy state estimates.

Figure 5 shows the tracking error of the forward and lateral velocity and the yaw rate from the two **MIMOC** policies and from **cMPC**. As shown in Fig. 5, with perfect state estimation the three controllers have small tracking errors with slightly less error for the model-based controller and slightly more tracking error for **MIMOC** without domain randomization. However, if the state estimates are noisy, the model-based controller performs the worst followed by **MIMOC** without domain randomization. This demonstrates the importance of domain randomization during training and that **MIMOC** may outperform **cMPC** in the real-world where state estimation is indeed noisy. As shown in Video 2, Mini-Cheetah did not fall from any of the controllers. Yet, with noisy state estimates, the model-based controller was less stable than **MIMOC**.

Performance under Different Terrain Friction. To compare **MIMOC** against **cMPC** under different terrain friction coefficients, we evaluate the performance of Mini-Cheetah with different yaw rate commands and friction coefficients in simulation (Cheetah-Software). We simulated 8 different friction coefficients ranging from 0.05 to 0.4 as shown in Fig. 6. For every friction coefficient, we command Mini-Cheetah to follow a certain yaw rate. Then, we increment the yaw rate command until the robot falls. For all friction coefficients, **MIMOC** was able to withstand higher yaw rate commands than it was trained with; it trained with a maximum yaw rate of 2.0 rad/s. **MIMOC** outperformed **cMPC** for friction coefficients below 0.25 but **cMPC** outperformed **MIMOC** for friction coefficients above 0.25. Video 3 shows **MIMOC** and **cMPC** in these simulations.

MIMOC on the MIT Humanoid. To show that **MIMOC** can be applied to other legged platforms, we tested the MIT Humanoid with **MIMOC** in IsaacGym. In the first simulation, we ran the policy on the MIT Humanoid and commanded it to walk in multiple directions. Figure 7 shows screenshots of the MIT Humanoid walking in IsaacGym and Video 4 shows the full simulation. As shown in Fig. 7 and Video 4, we could command the MIT Humanoid to walk in all directions separately and simultaneously. Note that the reference trajectories did not include instances where the robot was commanded in multiple directions. The scripted commands were designed to direct the robot to walk in one direction at a time. This shows us that **MIMOC** can generalize beyond

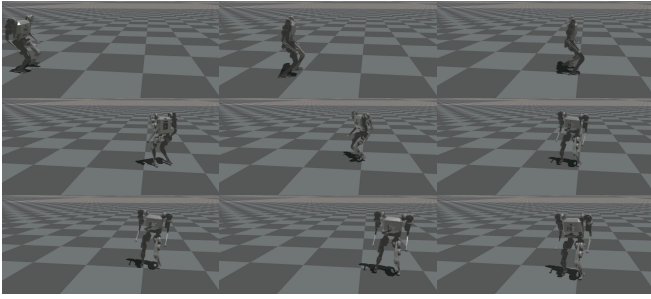


Fig. 7. This figure shows multiple screenshots of **MIMOC** on the MIT Humanoid. We can command the MIT Humanoid to walk in all directions separately and simultaneously, something not included in the reference trajectories and **MIMOC** was not trained for.

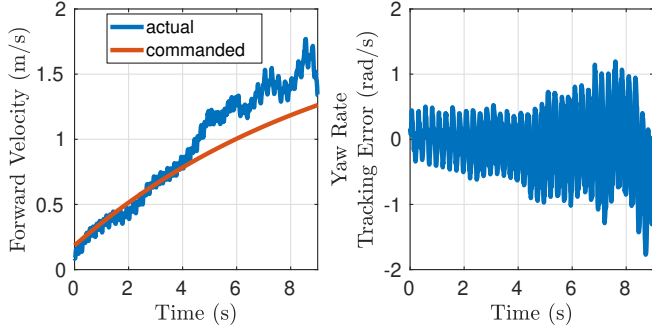


Fig. 8. The actual and commanded forward velocity (left) and the tracking error of the yaw rate (right). The figure shows the tracking performance of the MIT Humanoid walking using **MIMOC** and how fast it can walk.

the reference trajectories.

In another simulation, we evaluate how fast can the MIT Humanoid walk using **MIMOC**. To do so, we created a simulation where we command the robot to move forward with increasing forward velocity. The simulation starts with the robot stepping in-place and ends when the robot falls. Figure 8 shows the actual and forward velocity, and the tracking error of the yaw rate. As shown in Fig. 8, the robot was able to walk with a forward velocity exceeding 1 m/s. Over 1 m/s, the robot was still able to walk, but the tracking errors increased. In this simulation, the robot reached a maximum commanded forward velocity of 1.26 m/s.

Mini-Cheetah Outdoor Experiments. To evaluate the robustness of **MIMOC**, we tested it on Mini-Cheetah in several outdoor environments. Figure 1 shows screenshots of these experiments shown in more detail in Video 5. Mini-Cheetah with **MIMOC** traversed multiple terrains following user commands. We could also command Mini-Cheetah at different gait frequencies, something that **MIMOC** was not trained for. We also commanded Mini-Cheetah for higher velocities than in training. As shown in Video 5, another advantage of **RL** over **cMPC** is **MIMOC** does not go unstable if we suddenly lift Mini-Cheetah. If **cMPC** were lifted, the robot would suddenly go unstable and flail wildly. Finally, as shown in Video 5, Mini-Cheetah was able to traverse different terrains with different slopes and friction including grass, rocks, asphalt, mud, etc.

VI. LIMITATIONS AND FUTURE WORK

We identified several limitations of **MIMOC** that we are investigating for future work. First, although we randomized body pushes during training, we found that the recovery of the **RL** policy is only reactive. By this we mean that while the robot can reject some pushes, it is not able to reason about taking steps if it deviates substantially from the trained reference. Second, the references only include trajectories from locomotion over flat terrain, and the policy was also only trained on flat terrain. When we deployed **MIMOC** on the Mini-Cheetah in outdoor environments (see Fig. 1) the robot was able to walk over more challenging terrains, but we would like to explore better training for more task diversity. Third, our references only included commanding the robot in a single direction at a time. In simulation and experiment, **MIMOC** was able to generalize to higher speeds and in different directions simultaneously, but a more comprehensive dataset would likely improve performance.

To expand on this work and overcome these limitations, we are exploring two main ideas. One is to use **MIMOC** as a warm-started actor for more traditional reward-shaping and domain randomization. A second is to use our method to blend and fuse multiple references into a single policy, either by splicing incompatible references or by training a single policy to imitate the behaviors of multiple policies. We additionally plan to test **MIMOC** on the MIT Humanoid hardware.

VII. CONCLUSION

We presented **MIMOC**, an **RL** locomotion controller that learns by imitating model-based optimal controllers. **MIMOC** is trained to track reference trajectories provided by a model-based controller and follow user commands. **MIMOC** addresses some challenges faced by other motion imitation **RL** approaches. **MIMOC** does not require motion retargeting since the reference trajectories are designed for the robot, are dynamically feasible because they were captured in dynamic simulation, and include torque data which we showed to improve training and performance. **MIMOC** also overcomes some challenges faced by model-based optimal controllers since it is less sensitive to noisy state estimation because the policy is trained with domain randomization and noisy observations. Finally, **MIMOC** can be deployed on real robots like the Mini-Cheetah and transfers to other legged systems like the MIT Humanoid. We showed the robustness of **MIMOC** on the Mini-Cheetah in a wide range of challenging terrain including slopes, grass, asphalt, mud, etc.

MIMOC has three main outcomes. First, torque tracking is indeed essential for real-world deployment and faster learning convergence. Second, **RL** policies trained with **MIMOC** can outperform model-based optimal controllers when state estimation is noisy. Third, **MIMOC** trained with domain randomization can outperform model-based optimal controllers at low ground friction.

REFERENCES

- [1] J. Lee, J. Hwangbo, L. Wellhausen, V. Koltun, and M. Hutter, "Learning quadrupedal locomotion over challenging terrain," *Sci. Robot.*, vol. 5, no. 47, p. eabc5986, Oct. 2021, DOI:10.1126/scirobotics.abc5986.
- [2] C. Yang, K. Yuan, Q. Zhu, W. Yu, and Z. Li, "Multi-expert learning of adaptive legged locomotion," *Sci. Robot.*, vol. 5, no. 49, p. eabb2174, Dec. 2020, DOI:10.1126/scirobotics.abb2174.
- [3] C. Semini, V. Barasuol, M. Focchi, C. Boelens, M. Emara, S. Casella, O. Villarreal, R. Orsolino, G. Fink, S. Fahmi, G. Medrano-Cerda, and D. G. Caldwell, "Brief introduction to the quadruped robot HyQReal," in *Italian Conference on Robotics and Intelligent Machines (I-RIM)*, Rome, Italy, Oct. 2019, pp. 1–2.
- [4] B. Katz, J. Di Carlo, and S. Kim, "Mini cheetah: A platform for pushing the limits of dynamic quadruped control," in *Proc. IEEE Int. Conf. Robot. Automat. (ICRA)*, Montreal, QC, Canada, May 2019, pp. 6295–6301, DOI:10.1109/ICRA.2019.8793865.
- [5] G. Bledt, M. J. Powell, B. Katz, J. Di Carlo, P. M. Wensing, and S. Kim, "MIT Cheetah 3: Design and control of a robust, dynamic quadruped robot," in *Proc. IEEE/RSJ Int. Conf. Intell. Robot. Syst. (IROS)*, Madrid, Spain, Oct. 2018, pp. 2245–2252, DOI:10.1109/IROS.2018.8593885.
- [6] M. Hutter, C. Gehring, D. Jud, A. Lauber, C. D. Bellicoso, V. Tsounis, J. Hwangbo, K. Bodie, P. Fankhauser, M. Bloesch, R. Diethelm, S. Bachmann, A. Melzer, and M. Hoepflinger, "Anymal - a highly mobile and dynamic quadrupedal robot," in *Proc. IEEE/RSJ Int. Conf. Intell. Robot. Syst. (IROS)*, Daejeon, South Korea, Oct. 2016, pp. 38–44, DOI:10.1109/IROS.2016.7758092.
- [7] Boston Dynamics, Spot, 2021, <https://www.bostondynamics.com/spot>, [Online; accessed Jun. 2022].
- [8] Agility Robotics, Robots, 2021, <https://www.agilityrobotics.com/robots>, [Online; accessed Jun. 2022].
- [9] Unitree Robotics, Go1, 2021, <https://www.unitree.com/products/go1>, [Online; accessed Jun. 2022].
- [10] D. Kim, J. Di Carlo, B. Katz, G. Bledt, and S. Kim, "Highly dynamic quadruped locomotion via whole-body impulse control and model predictive control," in *arXiv preprint*, Sep. 2019, pp. 1–8. [Online]. Available: <https://arxiv.org/abs/1909.06586>
- [11] S. Fahmi, C. Mastalli, M. Focchi, and C. Semini, "Passive whole-body control for quadruped robots: Experimental validation over challenging terrain," *IEEE Robot. Automat. Lett. (RA-L)*, vol. 4, no. 3, pp. 2553–2560, Jul. 2019, DOI:10.1109/LRA.2019.2908502.
- [12] S. Kuindersma, F. Permenter, and R. Tedrake, "An efficiently solvable quadratic program for stabilizing dynamic locomotion," in *Proc. IEEE Int. Conf. Robot. Automat. (ICRA)*, Hong Kong, China, May 2014, pp. 2589–2594, DOI:10.1109/ICRA.2014.6907230.
- [13] J.-P. Sleiman, F. Farshidian, M. V. Minniti, and M. Hutter, "A unified mp framework for whole-body dynamic locomotion and manipulation," *IEEE Robot. Automat. Lett. (RA-L)*, vol. 6, no. 3, pp. 4688–4695, Mar. 2021, DOI:10.1109/LRA.2021.3068908.
- [14] G. Bledt and S. Kim, "Extracting legged locomotion heuristics with regularized predictive control," in *Proc. IEEE Int. Conf. Robot. Automat. (ICRA)*, Paris, France, May 2020, pp. 406–412, DOI:10.1109/ICRA40945.2020.9197488.
- [15] J. Di Carlo, P. M. Wensing, B. Katz, G. Bledt, and S. Kim, "Dynamic locomotion in the mit cheetah 3 through convex model-predictive control," in *Proc. IEEE/RSJ Int. Conf. Intell. Robot. Syst. (IROS)*, Madrid, Spain, Oct. 2018, pp. 1–9, DOI:10.1109/IROS.2018.8594448.
- [16] O. Melon, R. Orsolino, D. Surovik, M. Geisert, I. Havoutis, and M. Fallon, "Receding-horizon perceptive trajectory optimization for dynamic legged locomotion with learned initialization," in *Proc. IEEE Int. Conf. Robot. Automat. (ICRA)*, Xi'an, China (Virtual), Jun. 2021, pp. 9805–9811, DOI:10.1109/ICRA48506.2021.9560794.
- [17] B. Ponton, M. Khadiv, A. Meduri, and L. Righetti, "Efficient multi-contact pattern generation with sequential convex approximations of the centroidal dynamics," *IEEE Trans. Robot. (T-RO)*, vol. 37, no. 5, pp. 1661–1679, Feb. 2021, DOI:10.1109/TRO.2020.3048125.
- [18] C. Mastalli, R. Budhiraja, W. Merkt, G. Saurel, B. Hamoud, M. Naveau, J. Carpentier, L. Righetti, S. Vijayakumar, and N. Mansard, "Crocodyl: An efficient and versatile framework for multi-contact optimal control," in *Proc. IEEE Int. Conf. Robot. Automat. (ICRA)*, Virtual, May 2020, pp. 2536–2542, DOI:10.1109/ICRA40945.2020.9196673.
- [19] A. W. Winkler, C. D. Bellicoso, M. Hutter, and J. Buchli, "Gait and trajectory optimization for legged systems through phase-based end-effector parameterization," *IEEE Robot. Automat. Lett. (RA-L)*, vol. 3, no. 3, pp. 1560–1567, Feb. 2018, DOI:10.1109/LRA.2018.2798285.
- [20] N. Rudin, D. Hoeller, P. Reist, and M. Hutter, "Learning to walk in minutes using massively parallel deep reinforcement learning," in *Proc. Conf. Robot Learn. (CoRL)*, London, UK, Nov. 2021, pp. 91–100.
- [21] W. Yu, D. Jain, A. Escontrela, A. Iscen, P. Xu, E. Coumans, S. Ha, J. Tan, and T. Zhang, "Visual-locomotion: Learning to walk on complex terrains with vision," in *Proc. Conf. Robot Learn. (CoRL)*, London, UK, Nov. 2021, pp. 1291–1302.
- [22] T. Miki, J. Lee, J. Hwangbo, L. Wellhausen, V. Koltun, and M. Hutter, "Learning robust perceptive locomotion for quadrupedal robots in the wild," *Sci. Robot.*, vol. 7, no. 62, p. eabk2822, Jan. 2022, DOI:10.1126/scirobotics.abk2822.
- [23] S. Gangapurwala, M. Geisert, R. Orsolino, M. Fallon, and I. Havoutis, "Real-time trajectory adaptation for quadrupedal locomotion using deep reinforcement learning," in *Proc. IEEE Int. Conf. Robot. Automat. (ICRA)*, Xi'an, China (Virtual), Oct. 2021, pp. 1–7.
- [24] A. Kumar, Z. Fu, D. Pathak, and J. Malik, "RMA: Rapid motor adaptation for legged robots," in *Proc. Robot. Sci. and Syst. (RSS)*, Virtual, Jul. 2021, pp. 1–15, DOI:10.15607/RSS.2021.XVII.011Fe.
- [25] V. Tsounis, M. Alge, J. Lee, F. Farshidian, and M. Hutter, "Deepgait: Planning and control of quadrupedal gaits using deep reinforcement learning," *IEEE Robot. Automat. Lett. (RA-L)*, vol. 5, no. 2, pp. 3699–3706, Mar. 2020, DOI:10.1109/LRA.2020.2979660.
- [26] A. Iscen, K. Caluwaerts, J. Tan, T. Zhang, E. Coumans, V. Sindhwani, and V. Vanhoucke, "Policies modulating trajectory generators," in *Proc. Conf. Robot Learn. (CoRL)*, Zurich, Switzerland, Oct. 2018, pp. 916–926.
- [27] G. Ji, J. Mun, H. Kim, and J. Hwangbo, "Concurrent training of a control policy and a state estimator for dynamic and robust legged locomotion," *IEEE Robot. Automat. Lett. (RA-L)*, vol. 7, no. 2, pp. 4630–4637, Feb. 2022, DOI:10.1109/LRA.2022.3151396.
- [28] J. Siekmann, Y. Godse, A. Fern, and J. Hurst, "Sim-to-real learning of all common bipedal gaits via periodic reward composition," in *Proc. IEEE Int. Conf. Robot. Automat. (ICRA)*, Xi'an, China, May 2021, pp. 7309–7315, DOI:10.1109/ICRA48506.2021.9561814.
- [29] X. B. Peng, E. Coumans, T. Zhang, T.-W. Lee, J. Tan, and S. Levine, "Learning agile robotic locomotion skills by imitating animals," in *Proc. Robot. Sci. and Syst. (RSS)*, Corvallis, Oregon, USA, Jul. 2020, pp. 1–14, DOI:10.15607/RSS.2020.XVI.064.
- [30] L. Hasenclever, F. Pardo, R. Hadsell, N. Heess, and J. Merel, "CoMimic: Complementary task learning & mimicry for reusable skills," *Virtual*, Jul. 2020.
- [31] H. Zhang, S. Starke, T. Komura, and J. Saito, "Mode-adaptive neural networks for quadruped motion control," *ACM Trans. Graph.*, vol. 37, no. 4, pp. 1–11, Aug. 2018, DOI:10.1145/3197517.3201366.
- [32] X. B. Peng, P. Abbeel, S. Levine, and M. van de Panne, "Deepmimic: Example-guided deep reinforcement learning of physics-based character skills," *ACM Trans. Graph.*, vol. 37, no. 4, pp. 1–18, Aug. 2018, DOI:10.1145/3197517.3201311.
- [33] M. Chignoli, S. Morozov, and S. Kim, "Rapid and reliable quadruped motion planning with omnidirectional jumping," in *Proc. IEEE Int. Conf. Robot. Automat. (ICRA)*, May 2022, pp. 1–7.
- [34] H. Park, P. Wensing, and S. Kim, "High-speed bounding with the mit cheetah 2: Control design and experiments," *Int. J. Robot. Res. (IJRR)*, vol. 36, no. 2, pp. 167–192, Mar. 2017, DOI:10.1177/0278364917694244.
- [35] P. Wieber, *Holonomy and Nonholonomy in the Dynamics of Articulated Motion*. Berlin, Heidelberg: Springer Berlin Heidelberg, 2006, pp. 411–425, DOI:10.1007/978-3-540-36119-0.20.
- [36] S. Fahmi, G. Fink, and C. Semini, "On state estimation for legged locomotion over soft terrain," *IEEE Sens. Lett. (L-SENS)*, vol. 5, no. 1, pp. 1–4, Jan. 2021.
- [37] A. Babadi, K. Naderi, and P. Hämläinen, "Self-imitation learning of locomotion movements through termination curriculum," in *Motion, Interaction and Games (MIG)*, Newcastle upon Tyne, UK, Oct. 2019, pp. 1–7, DOI:10.1145/3359566.3360072.
- [38] Z. Li, X. Cheng, X. B. Peng, P. Abbeel, S. Levine, G. Berseth, and K. Sreenath, "Reinforcement learning for robust parameterized locomotion control of bipedal robots," in *Proc. IEEE Int. Conf. Robot. Automat. (ICRA)*, Xi'an, China, May 2021, pp. 2811–2817, DOI:10.1109/ICRA48506.2021.9560769.

- [39] P. Brakel, S. Bohez, L. Hasenclever, N. Heess, and K. Bousmalis, "Learning coordinated terrain-adaptive locomotion by imitating a centroidal dynamics planner," in *arXiv preprint*, Oct. 2021, pp. 1–10. [Online]. Available: <https://arxiv.org/abs/2111.00262>
- [40] M. Chignoli, D. Kim, E. Stanger-Jones, and S. Kim, "The mit humanoid robot: Design, motion planning, and control for acrobatic behaviors," in *Proc. IEEE/RAS Int. Conf. Humanoid Robot. (Humanoids)*, Munich, Germany, Jul. 2021, pp. 1–8, DOI:10.1109/HUMANOIDS47582.2021.9555782.
- [41] V. Makoviychuk, L. Wawrzyniak, Y. Guo, M. Lu, K. Storey, M. Macklin, D. Hoeller, N. Rudin, A. Allshire, A. Handa, and G. State, "Isaac gym: High performance gpu-based physics simulation for robot learning," in *arXiv preprint*, Aug. 2021, pp. 1–32. [Online]. Available: <https://arxiv.org/abs/2108.10470>
- [42] Cheetah-Software, <https://github.com/mit-biomimetics/Cheetah-Software>, [Online; accessed Jun. 2022].
- [43] R. S. Sutton and A. G. Barto, *Reinforcement Learning: An Introduction*, 2nd ed. Cambridge, MA, USA: MIT Press, 2018.
- [44] J. Schulman, F. Wolski, P. Dhariwal, A. Radford, and O. Klimov, "Proximal policy optimization algorithms," in *arXiv preprint*, Aug. 2017, pp. 1–12. [Online]. Available: <https://arxiv.org/abs/1707.06347>
- [45] A. Miller, S. Fahmi, M. Chignoli, and S. Kim, "MIMOC Accompanying Video," Youtube, May. 2023, https://youtu.be/fSR_mGezC4w. [Online; accessed May. 2023].